A practical consolidation solution based on the time-dependent discharge rate around PVDs

Yang Yu[1], Gang Wu[1, 2], Hongyue Sun[1], Xueyu Geng[2]*

(1. Ocean College, Zhejiang University, Zhoushan, Zhejiang 316021, China)

(2. School of Engineering, The University of Warwick, Coventry CV4 7AL, UK)

(*Corresponding author Xueyu Geng, Xueyu.Geng@warwick.ac.uk, School of Engineering, The University of Warwick, Coventry CV4 7AL, UK)

Abstract: This study presents a practical consolidation solution for ground improvement used prefabricated vertical drains (PVDs) by incorporating the available time-dependent discharge rate around PVDs, which can be easily obtained by laboratory test and field monitoring. Only radial consolidation is taken into account in the derivation to significantly simplify the final expression as the vertical consolidation can be neglected in a typical soft ground improvement project. The proposed solution is verified by the finite element method (FEM) and two case histories, including vacuum preloading and surcharge loading. The verification results show that the proposed solution can predict the development of excess pore water pressure (EPWP) and the degree of consolidation (DOC) effectively and accurately. Design charts and framework are developed to assist geotechnical engineers in using

this solution for field construction and performance prediction.

Keywords: axisymmetric consolidation; time-dependent discharge rate; equal-strain assumption; numerical simulation

Nomenclature

r, z radial and vertical coordinates

u, $\bar{u}_r$, u_r, u_0 excess pore water pressure (EPWP), average radial EPWP, virtual EPWP in the radial direction and initial average EPWP

C_v, C_h vertical and horizontal coefficients of consolidation

m_v volumetric compressibility

k_v, k_h, k_s vertical hydraulic conductivity and horizontal hydraulic conductivity within undisturbed zone, and horizontal hydraulic conductivity of smear soil

γ_w unit weight of water

t elapsed time

h, d_e, d thickness of soft soil, effective influence diameter of PVD and PVD spacing

E_s constrained modulus of the soil

ε_v volumetric strain

r_d, r_s, r_e radius of the equivalent cylinder of PVD, the smeared zone, and the effective influence zone of PVD

$q(t)$ time-dependent discharge rate around PVDs

A wetted cross-section area

$g(t)$ time-dependent EPWP gradient at $r = r_d$

c_s ratio between the horizontal hydraulic conductivity of soil within smear zone and undisturbed zone

n, s ratio between the radii of effective influenced zone and PVD and ratio between the radii of smear zone and PVD

U, U_t degree of consolidation (DOC) and modified DOC induced by multi-stage loading

s, s_c time-dependent settlement at any given time and the ultimate settlement

a, b width and thickness of band-shaped drainage board

t_{n-1}, t_n starting and ending time of each stage under a constant-speed loading process

$\Delta p'$, $\Delta p''$ loading increments that correspond to the first and second stages of loading

q_{w0} initial value or short-term value of the discharge rate around PVDs

A_0 coefficient with respect to the time-dependent discharge rate

Introduction

Civil engineering infrastructures are commonly constructed on weak soils that require improvement to resist applied loads [27, 31, 38, 48]. Improving soils in a time-efficient and cost-effective manner can not only ensure a safer, more reliable, efficient, sustainable, and resilient infrastructure but also offer great value to investors, contractors, and users [1, 4, 47, 34]. Prefabricated vertical drains (PVDs) are widely used in practice by creating short horizontal drainage paths to accelerate the process of soil consolidation [5, 8, 12, 22, 23, 39, 43, 45].

As a valuable factor to provide rational guidance on the effectiveness of soft ground improvement, the degree of consolidation (DOC) evaluated by field settlement measurement is widely used in the field. Nonetheless, the use of settlement measurement to estimate DOC could be problematic [17, 33, 35, 41]. Chu and Yan [16] indicated it is more suitable to predict DOC by utilizing pore pressure dissipation instead of settlement measurement due to the existing post-construction settlement during the primary consolidation. Currently, the pore pressure within the subsoil is measured by piezometers or pore pressure transducers which can cause some discrepancy [19].

During the PVD-assisted consolidation process, pore water can be squeezed out of soil under surcharge loading or sucked out through vacuum preloading, flows into and through PVDs, and then removed by pumps. Generally, the more water squeezed out from soil, the more water removed from PVDs by pumps due to the high discharge capacity of pumps. Thus, field and laboratory tests showed that soil consolidation behavior is associated with the variation of time-dependent discharge rate within PVDs [3, 14, 42]. According to aforementioned description of the relationship between time-dependent discharge and consolidation behavior, the prediction of DOC by adopting the time-dependent discharge rate around PVDs can be a potential complementary approach to predict the effectiveness of soft ground improvement by using settlement and pore pressure measurement.

A simplified solution is derived in this study to predict soil consolidation behavior with respect to the discharge rate around PVDs. Considering the fact that an accurate, time-dependent discharge rate of PVDs can be determined by laboratory experiment and field monitoring, the proposed solution can be used to predict actual soil consolidation behavior, then to instruct the geotechnical design and predict the consolidation behavior during the construction. The proposed analytical solution is verified by a comparison with a finite element model (FEM). At the end, this study presents two case histories to demonstrate its practical prediction to the field consolidation behavior. Furthermore, some actual design steps by using the proposed method and design charts are presented for its practical uses.

Consolidation Model

Governing equations

Governing equations are established based on an axisymmetric model for the soil consolidation with a single PVD penetrating the soil stratum completely shown in Figure 1. The axisymmetric model is based on the following assumptions:

(1) The soil unit cell has a constant thickness and is assumed to be homogeneous and saturated during the entire consolidation process.

(2) The seepage of pore water within the subsoil yields Darcy's law.

(3) The soil is subjected to a constant surcharge loading, which is applied instantaneously. The initial excess pore water pressure (EPWP) is uniform along the depth of the soil.

(4) The stress-strain relationship of the soil deposit is assumed to be linearly elastic during the entire consolidation process.

(5) The small stain assumption is valid on the unit cell.

(6) Deformation occurs on the vertical direction only, and the horizontal displacement is neglected. And the vertical deformation is caused by pore water pressure dissipation.

(7) One-way drainage unit cell is assumed herein, namely pervious boundary for top and impervious boundary for bottom of the unit cell.

(8) The soil deposit is fully saturated during the entire consolidation process with two phases, namely liquid and solid phases.

Based on these assumptions, the governing equations of consolidation of soil are presented as follows [2]:

$$\frac{\partial u}{\partial t} = C_v \frac{\partial^2 u}{\partial z^2} + C_h \left(\frac{\partial^2 u}{\partial r^2} + \frac{1}{r}\frac{\partial u}{\partial r}\right) \tag{1}$$

$$C_v = \frac{k_v}{m_v \gamma_w}, C_h = \frac{k_h}{m_v \gamma_w} \tag{2}$$

where r and z are the radial and vertical coordinates, respectively; u represents time-dependent EPWP; C_v and C_h are the vertical and horizontal coefficients of consolidation, respectively; m_v denotes the volumetric compressibility, and k_v and k_h are the vertical and horizontal hydraulic conductivity, respectively, which can be measured by laboratory or field tests [7, 40]; γ_w is the unit weight of water; and t is the elapsed time.

Orleach [36] concluded that vertical consolidation of soil can be neglected in most of the cases with PVDs, for example, when the time factor $T_v/T_h < 0.02$ (i.e., $T_v = C_v t/h^2$, $T_h = C_h t/d_e^2$, h and d_e are the thickness of soft soil and the effective influence diameter of PVD, respectively. $d_e = 1.05d$ when PVDs are arranged in a triangular pattern or d_e

= 1.13d when PVDs are arranged in a square pattern. d denotes the spacing between two adjacent PVDs). These parameters can be readily obtained in practice. For example, if PVDs are arranged in a triangular pattern with a typical spacing of 1.0 m ($d_e \approx$ 1.05 m) and the thickness of soil deposit is larger than 10 m, and the C_h and C_v values are assumed to be the same, then T_v/T_h would be less than 0.02. In most practices, the PVD-assisted ground technique is used to improve thick soft soil (h > 10 m). Moreover the C_v/C_h value is normally less than 1.0 [37]. Hence, the scenario of $T_v/T_h < 0.02$ is very common in actual practice and the vertical consolidation behavior is neglected in this study.

In general, the strain condition is assumed to be free-strain or equal-strain condition to solve a consolidation problem [6, 32, 44]. When flexible surcharge is applied on the ground surface, it will result in differential settlement at the surface. For this scenario, free-strain condition can be assumed. However, when rigid surcharge is applied on the ground surface, the surface settlement will be uniform. For this scenario, equal-strain condition can be assumed. To better stabilize the upper structure, the surface settlement should remain uniform [46]. As a result, the equal settlement is a basic requirement for PVD-assisted ground within the design scheme. According to Orleach's conclusion and equal-strain assumption, Eq. (1) can be simplified as [24, 25]:

$$\frac{\partial \bar{u}_r}{\partial t} = C_h\left(\frac{\partial^2 u_r}{\partial r^2} + \frac{1}{r}\frac{\partial u_r}{\partial r}\right) \tag{3}$$

where $\bar{u}_r$ and u_r are the average radial EPWP and virtual EPWP in the radial direction, respectively.

Based on the equal-strain assumption, the vertical strain along the radial direction of the soil is equal to its average value:

$$\frac{\partial \varepsilon_v}{\partial t} = -\frac{1}{E_s}\frac{\partial \bar{u}_r}{\partial t} \quad (4)$$

where E_s denotes the constrained modulus of the soil; ε_v represents the volumetric strain.

Eq. (4) is substituted into Eq. (3) after considering the smear effect to obtain the following governing equations:

$$-\frac{k_s}{\gamma_w}\frac{1}{r}\frac{\partial}{\partial r}\left(r\frac{\partial u_r}{\partial r}\right) = \frac{\partial \varepsilon_v}{\partial t}, r_d \le r \le r_s \quad (5a)$$

$$-\frac{k_h}{\gamma_w}\frac{1}{r}\frac{\partial}{\partial r}\left(r\frac{\partial u_r}{\partial r}\right) = \frac{\partial \varepsilon_v}{\partial t}, r_s \le r \le r_e \quad (5b)$$

where k_s is the horizontal hydraulic conductivity of the smeared soil; r_d, r_s, r_e represent the radii of the equivalent cylinder of PVD, the smeared zone, and the effective influence zone of the PVD, respectively, as shown in Figure 1.

Boundary and initial conditions

Three boundary conditions are established at $r = r_d$, $r = r_s$, and $r = r_e$. $r = r_d$ stands for the interface between the equivalent cylinder of PVD and the smeared soil. Note that as vertical consolidation is not taken into account in the present work, the effect of gravity on the discharge is ignored in the soil deposit and is taken account in the PVDs when well resistance exists. The discharge develops consistently along the length of the PVD during the consolidation process. Introducing the Dupuit assumption [21], the EPWP gradient at $r = r_d$ can be obtained:

$$\left.\frac{\partial u_r}{\partial r}\right|_{r=r_d} = \frac{q(t)\gamma_w}{k_s A} = g(t) \tag{6}$$

where $q(t)$ is the time-dependent discharge rate around PVDs; $A = 2\pi r_d h$ is the wetted cross-section area; and $g(t)$ represents the time-dependent EPWP gradient at $r = r_\mathrm{d}$.

$r = r_\mathrm{s}$ stands for the interface between the smeared soil and the undisturbed soil. The continuity of the flow rate at $r = r_\mathrm{s}$ can be described by:

$$k_s \left.\frac{\partial u_r}{\partial r}\right|_{r=r_s^-} = k_h \left.\frac{\partial u_r}{\partial r}\right|_{r=r_s^+} \tag{7}$$

$r = r_\mathrm{e}$ stands for an impervious boundary, beyond which the EPWP is not influenced by the PVD. The impervious boundary condition at $r = r_\mathrm{e}$ is described by:

$$\left.\frac{\partial u_r}{\partial r}\right|_{r=r_e} = 0 \tag{8}$$

Under the initial condition, it is assumed that the radial EPWP is equal to the constant initial average EPWP u_0, which equals to the magnitude of instantaneous surface surcharge loading. This initial condition can be expressed as follows:

$$\left.\bar{u}_r\right|_{t=0} = u_0 \tag{9}$$

Solutions

Double integrating Eq. (4) about r and introducing the boundary conditions expressed by Eqs. (6) to (8), the radial EPWP can be obtained as follows by assuming $c_\mathrm{s} = k_\mathrm{s}/k_\mathrm{h}$:

$$u_r = \left.u_r\right|_{r=r_s} - \frac{g(t) r_d}{r_e^2 - r_d^2}\left(r_e^2 \ln\frac{r_s}{r} - \frac{r_s^2 - r^2}{2}\right), r_d \le r \le r_s \tag{10a}$$

$$u_r = \left.u_r\right|_{r=r_s} + \frac{g(t) r_d}{r_e^2 - r_d^2} c_s \left(r_e^2 \ln\frac{r}{r_s} - \frac{r^2 - r_s^2}{2}\right), r_s \le r \le r_e \tag{10b}$$

It can be seen that the EPWP at $r = r_s$ is the only unknown variable in Eq. (10). To obtain its expression, the average radial EPWP is introduced, which is defined as:

$$\bar{u}_r = \frac{1}{\pi(r_e^2 - r_d^2)}\int_{r_d}^{r_e} 2\pi r u_r dr \tag{11}$$

Substituting Eq. (10) into Eq. (11), the average radial EPWP is obtained by integration, as presented in detail in Appendix A:

$$\bar{u}_r = u_r\big|_{r=r_s} + \frac{2g(t)r_d s^2}{n^2-1}F_a \tag{12}$$

where

$$F_a = f_n + f_s + f_0 \tag{13}$$

$$f_n = [c_s(\frac{n^2}{2s^2}\ln\frac{n}{s} + \frac{4s^2-3n^2}{8s^2}) + \frac{\ln s}{2s^2} + \frac{1-s^2}{4s^2}]\frac{n^2}{n^2-1} \tag{14}$$

$$f_s = \frac{1}{8}(1-c_s)\frac{s^2}{n^2-1} \tag{15}$$

$$f_0 = (\frac{1}{8s^2} - \frac{1}{4})\frac{1}{n^2-1} \tag{16}$$

where $n = r_e/r_d$, $s = r_s/r_d$.

Eq. (17) is obtained by integrating Eq. (5a) and (5b) on r.

$$\frac{\partial u_r}{\partial r} = \frac{\gamma_w}{2k_s}(\frac{r_e^2}{r} - r)\frac{\partial \varepsilon_v}{\partial t}, r_d \le r \le r_s \tag{17a}$$

$$\frac{\partial u_r}{\partial r} = \frac{\gamma_w}{2k_h}(\frac{r_e^2}{r} - r)\frac{\partial \varepsilon_v}{\partial t}, r_s \le r \le r_e \tag{17b}$$

By substituting $r = r_d$ into Eq. (17), the following equation is obtained based on Eqs. (4) and (6):

$$\frac{\partial \bar{u}_r}{\partial t} = -E_s\frac{2g(t)k_s}{\gamma_w r_d(n^2-1)} \tag{18}$$

Integrating Eq. (18) on t and introducing the initial condition of Eq. (9), the average

EPWP can be expressed as:

$$\bar{u}_r = u_0 - E_s \int_0^t \frac{2g(t)k_s}{\gamma_w r_d (n^2 - 1)} dt \tag{19}$$

Substituting Eq. (19) into Eq. (12), the EPWP at $r = r_s$ is obtained:

$$u_r\big|_{r=r_s} = u_0 - E_s \int_0^t \frac{2g(t)k_s}{\gamma_w r_d (n^2 - 1)} dt - \frac{2g(t) r_d s^2}{n^2 - 1} F_a \tag{20}$$

Substituting Eq. (20) to Eq. (10), the solutions for the radial EPWP at any arbitrary radial distance are obtained:

$$u_r = u_0 - F_c k_s \int_0^t g(t)dt - g(t) r_d [F_s + F(R)], r_d \le r \le r_s \tag{21a}$$

$$u_r = u_0 - F_c k_s \int_0^t g(t)dt - g(t) r_d [F_s + c_s F(R)], r_s \le r \le r_e \tag{21b}$$

$$F_c = \frac{2E_s}{\gamma_w r_d (n^2 - 1)} \tag{22}$$

$$F_s = \frac{2s^2 F_a}{n^2 - 1} \tag{23}$$

$$R = \frac{r}{r_d} \tag{24}$$

$$F(R) = \frac{n^2}{n^2 - 1} \ln \frac{s}{R} - \frac{s^2 - R^2}{2(n^2 - 1)} \tag{25}$$

Based on the definition of DOC, Eq. (19) can be used to calculate the DOC:

$$U = 1 - \frac{\bar{u}_r}{u_0} = \frac{F_c k_s}{u_0} \int_0^t g(t)dt \tag{26}$$

where U is the DOC.

The solution for the EPWP without considering the smear effect can be obtained by assuming $r_s = r_e$ in Eq. (21a) or assuming $r_s = r_d$ in Eq. (21b), and $k_s = k_h$ for both solutions. The DOC without a smear effect can be obtained by the aforementioned process.

As shown in the above procedure of derivation, the final solution has been significantly simplified; therefore, it can be used conveniently. In addition to typical parameters required for conventional consolidation theories, the time-dependent discharge rate around PVDs is required to estimate the consolidation behavior. As expected, the time-dependent discharge rate in PVDs is affected by the lateral stress around PVDs. There are various equipments reported in previous literature [3, 10] used to simulate the field stress state and then measure the discharge rate in PVDs in laboratory scale. According to the proposed solution incorporating the available measurement of time-dependent discharge rate in laboratory, the consolidation curve can be determined to instruct the geotechnical design of associated projects. The detailed procedure is presented in the section of discussion. Additionally, the proposed solution can also be used to predict the real-time development of EPWP and settlement by measuring directly and accurately with the assistance of some gauges (e.g., Groundwater Flowmeter) installed in the PVDs.

Verification

Comparison with numerical simulation

Figure 2 shows the numerical model established with ABAQUS. The yellow area is the undisturbed soil, and the gray area is the smeared zone. The radius of the smeared zone is assumed as $2r_d$ [26]. An elastic constitutive model is used in the numerical analysis. Table 1 shows the properties of the soft soil according to Rixner et al [37]. As the vertical consolidation is not considered in this study, the gravity is not applied on the numerical model. Thus, the flow rate in the numerical simulation around the nodes of the PVD remains consistent along the length of the PVD. To better display the numerical model, the thickness of the soil is set to be 50 cm (h = 50 cm). The influence radius r_e equals to 20 times of the equivalent radius of the PVD (i.e., r_d,) [13] which is defined according to one of the most commonly-used band-shaped drainage boards as [24, 25]:

$$r_d = \frac{a+b}{\pi} \tag{27}$$

where a and b are the width and thickness of the band-shaped drainage board and the geometric dimension of the most commonly-used band-shaped drainage board is 100 mm × 4 mm.

Impervious boundaries are created on the outer surfaces of the numerical model as shown in Figure 2. A 100 kPa instantaneous load is applied on the upper surface of the numerical model. Note that the discharge rate around PVDs is unknown during the consolidation process. If a specific time-dependent discharge rate is applied on the surface of the PVD, it is difficult for the numerical model to converge due to the specific time-dependent discharge rate is related to many factors, such as lateral pressure, hydraulic conductivity in smeared zone and the permeability at the interface between PVDs and soil, and normally the development of discharge rate may not be applied on numerical model directly. Therefore, to obtain the time-dependent discharge rate and verify the proposed solution, the EPWP around PVDs is assumed to be 0 kPa during the simulation of the consolidation process and the flow rate at the node of PVD can be recorded in calculation.

Figure 3 shows the development of the settlement versus the radial distance of the measuring point from the center of the PVD. It is shown that the settlements at 30, 60, and 100 days are approximately uniform at different distances from the center of the PVD. This result implies that the equal-strain assumption is suitable for the consolidation of soil with PVDs.

Figure 4 shows the variation of flow rate around PVDs with time. The flow rate decreases exponentially with time. Substituting these rates into Eq. (21) yields the development of EPWP in the radial direction. Figure 5 shows the comparison between the simulated and calculated normalized EPWP in the radial direction by FEM and the solution proposed in this study, respectively. Good agreements are obtained between the simulated and calculated results for the model. Figure 5 shows that the EPWP increases with the increase of distance from the center of the PVD. With an increase of the time, the difference in the EPWP from the center to a certain distance becomes negligible. Also, the difference between the simulated and calculated results decreases. From Figure 5, it can be concluded that the proposed solution can well predict the variation of EPWP at different distances from the center of the PVD during the entire process of consolidation.

To obtain the DOC by the numerical simulation, the settlement at 100 years is first simulated by the numerical model and considered as the ultimate settlement of the model. The simulated DOC of the model at any time can be calculated by:

$$U = \frac{s}{s_c} \tag{28}$$

where s and s_c are the settlement at any time and the ultimate settlement, respectively.

Figure 6 compares the simulated and calculated DOC, which are in good agreement. It can be observed that the proposed solution slightly underestimated the DOC as compared with the simulated result at the initial time. Their difference becomes smaller with an increase of the time. The overall relative error does not exceed 10%. This comparison also proves that the proposed solution can well predict the consolidation behavior of the soft soil as that in the FEM model.

Comparison with field tests

Case A

A well-documented case history involving a fill embankment at the Saga Airport in Japan was reported by Chai et al [9]. This airport was constructed on a reclaimed land close to the Ariake Bay. The deposit consists of a weathered crust, a sand layer and soft and highly-compressible clay. Table 2 presents the thicknesses and properties of the soil strata.

PVDs were installed at a depth of approximately 25 m in a square pattern with a spacing of 1.5 m. The cross-sectional dimension of each PVD is 100 mm × 4 mm. The fill was placed at a rate of approximately 0.03 m/day for multiple stages, which can be modeled as multi-ramp loading. The first filling lasted 18 days. After 72-day suspension, the second filling took 116 days. When the fill height reached 3.5 m, the filling stopped for 194 days. The unit weight of the fill material was 20 kN/m^3, and the final applied pressure on the ground surface was 70 kPa. Figure 7 shows the cross section of the embankment and the instrumentation locations in the field. As shown in

Table 2, AC2 was the thickest soil layer in this cross section and would dominate the consolidation process. Moreover, the PVDs penetrated the AC2 layer completely. To simplify the calculation, only the AC2 layer was considered in this study.

Figure 8 shows the flow rate around the PVD with time. The time-dependent flow rate was obtained by physical modeling tests in the laboratory to simulate the field condition. This figure illustrates that the time-dependent flow rate decreased exponentially with time. The fitting relationship between the flow rate of the PVD and time was obtained by the regression method as $v = 0.0282\exp(-0.0159\times t)$ ($R^2 = 0.9777$). The DOC under instantaneous loading can be obtained by substituting the fitting curve expression into Eq. (26).

The construction of the embankment could be divided into two stages, which were modeled as surcharge loading on the ground surface in two stages. The Terzaghi equation can be modified to calculate the DOC in each stage as follows [18]:

$$U_t = \sum_1^n U_{(t-\frac{t_n+t_{n+1}}{2})} \frac{\Delta p_n}{\sum \Delta p} \tag{29}$$

where U_t is the modified DOC; t_{n-1} and t_n are the starting and ending time of each stage under a constant-speed loading process, respectively. Since two stages of surcharge loading were used in this case history, the modified DOC can be calculated as follows:

when $0 < t < t_1$
$$U_t = U_{(\frac{t}{2})} \frac{\Delta p'}{\sum \Delta p} \tag{30}$$

when $t_1 < t < t_2$
$$U_t = U_{(t-\frac{t_1}{2})} \frac{\Delta p_1}{\sum \Delta p} \tag{31}$$

when $t_2 < t < t_3$

$$U_t = U_{(t-\frac{t_1}{2})} \frac{\Delta p_1}{\sum \Delta p} + U_{(\frac{t-t_1}{2})} \frac{\Delta p''}{\sum \Delta p} \tag{32}$$

when $t_3 < t < t_4$

$$U_t = U_{(t-\frac{t_1}{2})} \frac{\Delta p_1}{\sum \Delta p} + U_{(t-\frac{t_2+t_3}{2})} \frac{\Delta p''}{\sum \Delta p} \tag{33}$$

where $\Delta p'$ and $\Delta p''$ are the loading increments that correspond to the first and second stages of loading, respectively.

Figure 9 illustrates the comparison on settlement and EPWP calculated by proposed solution with field measurement and the prediction using other solutions. The Hansbo's consolidation theory [25] is one of the most commonly-used solutions in the practice, which is simplified with reasonable assumptions. Deng et al [20] proposed a rigorous analytical solution for consolidation of soil with PVDs at a changing drain resistance. The calculated settlement was computed using Eq. (28), in which the ultimate settlement was determined according to the measured data from the field. Table 2 and Figure 9 show the associated soil parameters for the AC2 layer which is required in Eqs. (21) to (26). Both the Hansbo's solution and Deng et al's solution were applied herein by using the same modified Terzaghi method as used in proposed solution for stage loading. Chai and Miura [10] used FEM to simulate the entire process of surcharge loading for this project and the EPWP was obtained. It can be illustrated from Figure 9 that the settlement increased rapidly during the surcharge loading. The increase rate of the settlement became slow after the completion of fill loading. It can be seen from Figure 9 that the settlement obtained by proposed solution is consistent with field measurement. Thus it can be concluded that the proposed solution can accurately predict the settlement.

By comparing the settlement results with other solutions, it illustrated that the proposed solution is identical with Deng et al's solution and numerical simulation results by Chai and Miura [10]. Due to high simplification and limitation of Hansbo's consolidation solution, the settlement results obtained by Hansbo's consolidation solution exhibit some discrepancy compared with field measurement and other solutions. Deng et al's solution assumes the varying well resistance in PVDs which can predict the development of settlement with sufficient accuracy, whereas the varying well resistance is expressed with an approximated formula by regression summarized by laboratory experimental results. As a result, the overall development of settlement deviates from the field measurement with acceptable error. Moreover, similar to other rigorous analytical solutions, Deng et al's solution is difficult to apply by geotechnical engineers due to its complexity of the equations and required parameters. The numerical simulation results by FEM are close to the proposed solution and field measurement. However, according to the complexity of field project, the modeling process is complicated and time-consuming. By comparing with other solutions, it can be concluded that the proposed solution can be an alternative with acceptable accuracy and simplification in predicting the development of settlement.

Figure 9 also shows the comparison of EPWP with other solutions. The EPWP was measured at the location of 5 m away from the center line of PVDs and 6 m below the ground surface. Although the calculated EPWP by proposed solution was lower than that the measured one, the distributions of the EPWP obtained by the proposed solution and measurement are similar. This difference may result from the inhomogeneous soil layer and possible measurement errors in the field.

Even though it is quite different from the measured value, the EPWP calculated by the proposed solution is in good agreement with those by the rigorous solution and the FEM before the surcharge load reaches the maximum. The above discussion demonstrates that the proposed solution, even though is highly simplified, can be conveniently used to predict the consolidation behavior of soft soil with PVDs for field applications with good accuracy.

Case B

Chu and Yan [16] reported a road embankment built on soft soil deposit at Tianjin Port in China. The thickness of the soil deposit was approximately 20 m. The soft clay at the depth of 5 to 6 m was reclaimed recently using clay slurry dredged from seabed. The clay below the reclaimed layer is original seabed clay. To rapidly increase the strength of the soil layer, the vacuum preloading technique was utilized. Field implementation was used in two sections (namely Section I and Section II). The details of the soil properties and construction procedure are well documented in the literature [15]. Figure 10 shows the schematic diagram of this project, which consists of a road section of 364.5 m long and 51 m wide. A vacuum pressure of 80 kPa was applied continuously for 90 days to compress the soft soil deposit.

The vacuum pressure increasing from 0 to 80 kPa in a very short period could be considered as instantaneous and uniform loading. The Hansbo's solution could not be applied in this case history as Hansbo's consolidation theory is based on the assumption of instantaneous and uniform fill loading subjected on the subsoil. However, the time-dependent discharge rate around PVDs increases with the existence of vacuum pressure. In the absence of time-dependent measurement of discharge in PVDs, back analysis was carried out to evaluate the development of discharge. According to the EPWP measurement, the development of discharge rate was obtained by utilizing Eq. (21). Then the obtained time-dependent discharge rate was substituted into Eq. (26) to calculate the DOC with time. The real-time settlement was estimated based on the ultimate settlement calculated by the Asaoka method using the monitored settlement data and the DOC with time.

Figure 11 shows the settlement and the EPWP reduction calculated by the proposed solution as compared with the measured results in Section I and II. Even though there are some differences, the proposed solution reasonably predicted the settlement and the EPWP reduction in this project. As the ultimate settlements measured in different sections are different (the ultimate settlements are 1.0 m in Section I and 1.2 m in Section II, respectively), the development of settlement calculated by proposed solution is different. And the soil profile is basically the same in both sections, and thus the calculated EPWP in different sections is on the same curve. Due to some novel ground treatment methods are proposed during the recent decades, some conventional analytical solutions may not be adaptive in these new techniques. However, when the time-dependent discharge rate is available and accurate, the precise prediction can be achieved by utilizing the proposed solution. As the prediction by proposed solution is consistent with field measurement, it can be concluded that the proposed solution is a potential alternative in geotechnical design of PVD-assisted ground.

Discussion

To apply the proposed solution to field implementation and monitoring, a parametric analysis should be conducted to obtain the DOC and time factor curve. Then the design charts are prepared to make reasonable design and instruct field construction. According to Deng et al. [19], the discharge rate around PVDs can be expressed as follows:

$$q(t) = q_{w0} \exp(-A_0 t) \tag{34}$$

where q_{w0} is the initial value or short-term value of the discharge rate around PVDs; A_0 is the coefficient with respect to the time-dependent discharge rate.

DOC is one of the critical parameters for design of an entire consolidation process. The DOC can be expressed as follows by incorporating Eqs. (6) (26) (34) and then integrating the incorporated formula.

$$U = \frac{F_c}{u_0} \frac{q_{w0}\gamma_w}{A} \frac{1}{A_0}[1 - \exp(-A_0 t)] \tag{35}$$

Generally, the expression for DOC is comprised with the time factor T_h ($T_h = C_h t/d_e^2$). Thus to analyze the influence of coefficient A_0, a dimensionless factor α is introduced herein and expressed as follows:

$$\alpha = A_0 \frac{d_e^2}{C_h} \tag{36}$$

When time becomes infinite, the DOC is 100%. Thus, the DOC can be expressed as a well-known formula, which is show as follows:

$$U = 1 - \exp(-\alpha T_h) \tag{37}$$

Figure 12 illustrates the development of DOC with the time factor. To obtain the time needed for a specific DOC, the dimensionless factor α is required to be determined. Based on the fact that the DOC is equal to 100% when time is infinite, the dimensionless factor α can be derived as follows:

$$\alpha = \frac{4n^2 q_{w0}\gamma_w}{\pi k_h (n^2 - 1) u_0 h} \approx \frac{4 q_{w0}\gamma_w}{\pi k_h u_0 h} \tag{38}$$

Under field conditions, the parameters q_{w0} and k_h are often variable due to the nature of soil deposit and measurement errors. Their variability should be considered in design. The mean horizontal hydraulic conductivity is assumed to be 2×10^{-8} m/s here according to the literature [14], and the coefficient of variation is assumed to be 0.5. The mean q_{w0} is assumed to be 3×10^{-8} m^3/s, and its coefficient of variation is assumed to be 0.5 [28–30, 49]. These two parameters are assumed to have Gamma distributions. Figure 13 and Figure 14 show the ranges of the dimensionless factor α. Obviously, if there are more detailed measurements of aforementioned parameters determined by field and laboratory tests, the distribution of the dimensionless factor α may be more rational to instruct the geotechnical design. In practical process without available parameters, an arrangement of PVDs is first assumed and the uncertain parameters are assumed to be distributed in a typical statistical model based on the mean value and standard deviation summarized in previous references. Then a most possible factor α can be determined according to the density of scatter points(e.g. Figure 13 and 14). Simultaneously, the consolidation curve can be determined when the factor α is obtained. According the obtained consolidation curve, the target of consolidation can be estimated to optimize the arrangement of PVDs by repeating aforementioned process If the curve for the deterministic dimensionless factor is not available in Figure 12, a linear interpolation could be conducted to determine the curve, which will be used to determine the time factor T_h required for the target DOC. According the obtained consolidation curve, the target of consolidation can be estimated to optimize the arrangement of PVDs by repeating aforementioned process.

In summary, to apply the proposed solution in this study, the following framework is suggested:

Step 1: Define the target DOC at a certain time period based on project requirements.

Step 2: Select a PVD pattern and improvement approach (e.g., fill preloading or vacuum preloading) and determine a loading procedure (e.g., single or staged loading).

Step 3: Measure relevant parameters by field surveying and laboratory tests, including the geometric features of soil and PVD properties, for instance, the initial or short-term value of the discharge rate around PVDs, the geometric dimension of PVD, the hydraulic conductivity of soil, and the thickness of the soil stratum.

Step 4: Based on Eq. (38), the factor α is obtained to determine the associated DOC – time factor curve according to Figure 12. If some properties cannot be determined accurately, such as the hydraulic conductivity of soil, a specific range of α can be determined according to the obtained initial or short-term discharge rate around PVDs from Figure 13 and Figure 14, and then assume a most possible factor α according to the density of scatter points.

Step 5: Based on the obtained specific factor α, the associated DOC – time factor curve is used to calculate the dimensionless time factor T_h for the soil deposit to reach the target DOC. If the obtained factor α is not available in Figure 12, linear interpolation should be carried out to obtain the required DOC – time factor curve. Find the corresponding time factor under the target DOC and then determine PVD spacing.

Step 6: In the field, the real-time discharge rate around PVDs, EPWP within the soil deposit and settlement are monitored to assess the actual consolidation behavior. The development of the consolidation process can be predicted by substituting the time-dependent discharge rate into the proposed solution. The proposed solution based on the discharge rate around PVDs can be a complementary approach to better describe the consolidation behavior. If the trend of the predicted consolidation process cannot reach the target, modify the loading process to redesign the consolidation process.

Conclusions

This study presents a practical solution for the consolidation of soft soil deposit with a single PVD based on the discharge boundary condition around PVDs under equal-strain assumption. The solution can predict EPWP and DOC of soft soil improved with PVDs. The comparisons of the proposed solutions with numerical simulation and measured data in two case histories verified the applicability and accuracy of the proposed solutions. Following conclusions can be made from this study:

(1) An axisymmetric consolidation solution based on the discharge boundary condition around PVDs under equal-strain assumption is proposed in this study. The prediction of the EPWP and the DOC can be determined by substituting the time-dependent discharge rate around PVDs into the proposed analytical solution.

(2) Numerical simulation is performed by FEM to simulate the consolidation behavior of a soft soil deposit with a single PVD. As the discharge around PVDs remains unknown during the entire consolidation process, the idealized consolidation behavior without well resistance was simulated to determine the time-dependent discharge rate around PVDs. The relationship between the discharge rate around PVDs and the consolidation time obtained by FEM simulation is substituted into the proposed analytical solution. The results show that the DOC and EPWP calculated by the proposed solution are in good agreement with the simulated results.

(3) Two case histories were used to evaluate the proposed analytical solution. The comparisons show that the settlement-time curve obtained by the proposed solution is in good agreement with the measured data. The proposed solution can be applied in various kinds of soft ground improvement techniques, including surcharging loading and vacuum preloading, with available time-dependent discharge rate around PVDs.

(4) Design charts for the relationship between the initial short-time discharge rate and the dimensionless factor α are developed to help choose the range of the dimensionless factor α and the most possible dimensionless factor α, which can be used to determine the consolidation curve. Based on the target DOC and obtained the

consolidation curve, the required design parameters can be determined. On the other hand, the real-time consolidation behavior can be predicted based on proposed solution by utilizing the field discharge measurement monitored by gauges. The proposed solution can be a potential complementary approach to the prediction of consolidation behavior by utilizing settlement and pore pressure measurement in field.

Acknowledgments

This study was sponsored by the Key R&D project of Zhejiang Province (2017C03006) and Zhejiang Provincial National Science Foundation of China (LQ17D020001).

Appendix A

Assume $n = r_e/r_d$, $s = r_s/r_d$ and $R = r/r_d$. The average radial EPWP can be obtained by combining Eqs. (10) and (11) as follows:

$$\bar{u}_r = u_r\big|_{r=r_s} + 2r_d\left[\int_1^s -\frac{g(t)R}{(n^2-1)^2}\left(n^2\ln\frac{s}{R}-\frac{s^2-R^2}{2}\right)dR + \int_s^n \frac{g(t)R}{(n^2-1)^2}c_s\left(n^2\ln\frac{R}{s}-\frac{R^2-s^2}{2}\right)dR\right] \quad (A1)$$

The second part of Eq. (A1) can be rewritten as Eqs. (A2) and (A3) as follows:

$$2r_d\int_1^s -\frac{g(t)R}{(n^2-1)^2}\left(n^2\ln\frac{s}{R}-\frac{s^2-R^2}{2}\right)dR \quad (A2)$$

$$2r_d\int_s^n \frac{g(t)R}{(n^2-1)^2}c_s\left(n^2\ln\frac{R}{s}-\frac{R^2-s^2}{2}\right)dR \quad (A3)$$

Eq. (A4) can be obtained by integrating Eq. (A2) as follows:

$$-\frac{2g(t)r_d}{(n^2-1)^2}\int_1^s R\left(n^2\ln\frac{s}{R}-\frac{s^2-R^2}{2}\right)dR \quad (A4)$$

$$-\frac{2g(t)r_d}{(n^2-1)^2}\int_1^s [n^2(\ln s-\ln R)R-\frac{s^2-R^2}{2}R]dR \tag{A5}$$

$$-\frac{2g(t)r_d}{(n^2-1)^2}[\frac{n^2(s^2-1)}{2}\ln s-n^2(\frac{s^2}{2}\ln s-\frac{s^2}{4}+\frac{1}{4})-\frac{s^2}{2}\frac{s^2-1}{2}+\frac{s^4-1}{8}] \tag{A6}$$

$$-\frac{2g(t)r_d}{(n^2-1)^2}(-\frac{n^2}{2}\ln s+n^2\frac{s^2-1}{4}-\frac{s^4-s^2}{4}+\frac{s^4-1}{8}) \tag{A7}$$

$$\frac{g(t)r_d}{(n^2-1)^2}[n^2\ln s-\frac{n^2}{2}(s^2-1)+\frac{(s^2-1)^2}{4}] \tag{A8}$$

Eq. (A9) can be obtained by integrating Eq. (A3) as follows:

$$\frac{2g(t)r_d}{(n^2-1)^2}c_s\int_s^n R(n^2\ln\frac{R}{s}-\frac{R^2-s^2}{2})dR \tag{A9}$$

$$\frac{2g(t)r_d}{(n^2-1)^2}c_s\int_s^n [n^2(\ln R-\ln s)R-\frac{R^2-s^2}{2}R])dR \tag{A10}$$

$$\frac{2g(t)r_d}{(n^2-1)^2}c_s[n^2(\frac{n^2}{2}\ln n-\frac{n^2}{4}-\frac{s^2}{2}\ln s+\frac{s^2}{4})-\frac{n^2(n^2-s^2)}{2}\ln s-\frac{n^4-s^4}{8}+\frac{s^2}{2}\frac{n^2-s^2}{2}] \tag{A11}$$

$$\frac{2g(t)r_d}{(n^2-1)^2}c_s(\frac{n^2s^2}{2}+\frac{n^4}{2}\ln\frac{n}{s}-\frac{3n^4+s^4}{8}) \tag{A12}$$

$$\frac{g(t)r_d}{(n^2-1)^2}c_s(n^4\ln\frac{n}{s}-\frac{3n^4+s^4-4n^2s^2}{4}) \tag{A13}$$

The average radial EPWP can be obtained by combining Eqs. (A1), (A8), and (A13) as follows:

$$\bar{u}_r = u_r\big|_{r=r_s}+\frac{2g(t)r_d s^2}{n^2-1}F_a \tag{A14}$$

where

$$F_a = f_n + f_s + f_0 \tag{A15}$$

$$f_n = [c_s(\frac{n^2}{2s^2}\ln\frac{n}{s}+\frac{4s^2-3n^2}{8s^2})+\frac{\ln s}{2s^2}+\frac{1-s^2}{4s^2}]\frac{n^2}{n^2-1} \tag{A16}$$

$$f_s = \frac{1}{8}(1-c_s)\frac{s^2}{n^2-1} \quad \text{(A17)}$$

$$f_0 = (\frac{1}{8s^2} - \frac{1}{4})\frac{1}{n^2-1} \quad \text{(A18)}$$

References

[1] Aoyama K, Yoshida T, Kamitani T. An alternative of soil scarification treatment for forest restoration: effects of soil replacement. J Forest Res-Jpn 2017;14(1):58-62.

[2] Barron RA. Consolidation of fine-grained soils by drain wells. Transactions of the American Society of Civil Engineers 1948;113(1):718-742.

[3] Bo MW. Discharge capacity of prefabricated vertical drain and their field measurements. Geotext Geomembranes 2004;22(1-2):37-48.

[4] Cai Y, Qiao H, Wang J, Geng X, Wang P, Cai Y. Experimental tests on effect of deformed prefabricated vertical drains in dredged soil on consolidation via vacuum preloading. Eng Geol 2017;222:10-19.

[5] Cai Y, Qiao H, Wang J, Geng X, Wang P, Cai Y. Experimental tests on effect of deformed prefabricated vertical drains in dredged soil on consolidation via vacuum preloading. Eng Geol 2017;222:10-19.

[6] Cargill KW. Prediction of consolidation of very soft soil. Journal of Geotechnical Engineering 1984;110(6):775-795.

[7] Chai J, Agung PMA, Hino T, Igaya Y, Carter, JP. Estimating hydraulic conductivity from piezocone soundings. Géotechnique 2011;61(8):699-708.

[8] Chai J, Bergado DT, Shen S. Modelling prefabricated vertical drain improved ground in plane strain analysis. Ground Improvement, ICE Proceedings 2013;166(GI2):65-77.

[9] Chai J, Miura N, Sakajo S, Bergado D. Behavior of vertical drain improved subsoil under embankment loading. Soils Found 1995;35(4):49-61.

[10] Chai J, Miura N. Investigation of factors affecting vertical drain behavior. J Geotech Geoenviron 1999;125(3):216-226.

[11] Chai J, Shen S, Miura N, Bergado DT. Simple method of modeling PVD-improved subsoil. J Geotech Geoenviron 2001;127(11):965-972.

[12] Chen J, Shen S, Yin Z, Xu Y, Horpibulsuk S. Evaluation of effective depth of PVD improvement in soft clay deposit: a field case study. Marine Georesources and Geotechnolgy 2016;34(5):420-430.

[13] China Academy of Building Research. Chinese technical code for ground improvement for buildings (JGJ 79-2002). China Architecture and Building Press Beijing; 2002.

[14] Chu J, Bo MW, Chang MF, Choa V. Consolidation and permeability properties of Singapore marine clay. J Geotech Geoenviron 2002;128(9):724-732.

[15] Chu J, Yan S, Yang H. Soil improvement by the vacuum preloading method for an oil storage station. Géotechnique 2000;50(6):625-632.

[16] Chu J, Yan SW. Estimation of degree of consolidation for vacuum preloading projects. Int J Geomech 2005;5(2):158-165.

[17] Cosenza P, Korošak D. Secondary consolidation of clay as an anomalous

diffusion process. Int J Numer Anal Met 2014;38(12):1231-1246.

[18] Das BM. Advanced soil mechanics. New York: CRC Press; 2013.

[19] Deng Y, Liu G, Lu M, Xie K. Consolidation behavior of soft deposits considering the variation of prefabricated vertical drain discharge capacity. Comput Geotech 2014;62:310-316.

[20] Deng Y, Xie K, Lu M. Consolidation by vertical drains when the discharge capacity varies with depth and time. Comput Geotech 2013;48:1-8.

[21] Dupuit J. Etudes Théoriques et Pratiques sur le mouvement des Eaux dans les canaux découverts et à travers les terrains perméables. Paris: Dunod; 1983.

[22] Fu H, Fang Z, Wang J, Chai J, Cai Y, Geng X, et al. Experimental comparison of electroosmotic consolidation of Wenzhou dredged clay sediment using intermittent current and polarity reversal. Mar Georesour Geotec 2018;36(1):131-138.

[23] Geng X, Yu HS. A large-strain radial consolidation theory for soft clays improved by vertical drains. Géotechnique 2017;67(11):1020-1028.

[24] Hansbo S, Jamiolkowski M, Kok L. Consolidation by vertical drains. Géotechnique 1981;31(1):45-66.

[25] Hansbo S. Consolidation of clay by band-shaped prefabricated drains. Ground Engineering 1979;12(5):16-25.

[26] Hansbo S. Foundation engineering: Newnes; 1994.

[27] Hegde A, Sitharam TG. Experiment and 3D-numerical studies on soft clay bed reinforced with different types of cellular confinement systems. Transportation

Geotechnics 2017;10:73-84.

[28] Hong HP, Shang JQ. Probabilistic analysis of consolidation with prefabricated vertical drains for soil improvement. Can Geotech J 1998;35(4):666-677.

[29] Hong HP. An efficient point estimate method for probabilistic analysis. Reliability Engineering and System Safety 1998;59(3):261-267.

[30] Hong HP. One-dimensional consolidation with uncertain properties. Can Geotech J 1992;29(1):161-165.

[31] Khemissa M, Mekki L, Mahamedi A. Laboratory investigation on the behaviour of an overconsolidated expansive clay in intact and compacted states. Transportation Geotechnics 2018;14:157-168.

[32] Leo CJ. Equal strain consolidation by vertical drains. J Geotech Geoenviron 2004;130(3):316-327.

[33] Li AL, Rowe K. Effects of viscous behavior of geosynthetic reinforcement and foundation soils on the performance of reinforced embankments. Geotext Geomembranes 2008;26(4):317-334.

[34] Ma L, Shen S, Luo C, Xu Y. Field evaluation on strength increase of soft structured clay under stage-constructed embankment. Marine Georesources and Geotechnology 2011;29(4):317-332.

[35] Ni P, Xu K, Mei G, Zhao Y. Effect of vacuum removal on consolidation settlement under a combined vacuum and surcharge preloading. Geotext Geomembranes 2019;47(1):12-22.

[36] Orleach P. Techniques to evaluate the field performance of vertical drains:

Massachusetts Institute of Technology; 1983.

[37] Rixner JJ, Kraemer SR, Smith AD. Prefabricated vertical drains: Engineering guidelines. Washington, D.C.: Federal Highway Administration; 1986.

[38] Rondonuwu SG, Chai J, Cai Y, Wang J. Prediction of the stress state and deformation of soil deposit under vacuum pressure. Transportation Geotechnics 2016;6:75-83.

[39] Shen S, Chai J, Hong Z, Cai F. Analysis of field performance of embankments on soft clay deposit with and without PVD-improvement. Geotextiles and Geomemberanes 2005;23(6):463-485.

[40] Shen S, Wang J, Wu H, Xu Y, Ye G, Yin Z. Evaluation of hydraulic conductivity for both marine and deltaic deposits based on piezocone testing. Ocean Engineering 2015;110:174-182.

[41] Shi J, Qian S, Zeng LL, Bian X. Influence of anisotropic consolidation stress paths on compression behaviour of reconstituted Wenzhou clay. Géotechnique Letters 2015;5(4):275-280.

[42] Tran-Nguyen HH, Edil TB, Schneider JA. Effect of deformation of prefabricated vertical drains on discharge capacity. Geosynth Int 2010;17(6):431-442.

[43] Wang J, Ma J, Liu F, Mi W, Cai Y, Fu H, et al. Experimental study on the improvement of marine clay slurry by electroosmosis-vacuum preloading. Geotext Geomembranes 2016;44(4):615-622.

[44] Wang XS, Jiao JJ. Analysis of soil consolidation by vertical drains with double porosity model. Int J Numer Anal Met 2004;28(14):1385-1400.

[45] Wu H, Shen S, Ma L, Yin Z, Horpibulsuk S. Evaluation of the strength increase of marine clay under staged embankment loading: a case study. Marine Georesources and Geotechnology 2015;33(6):532-541.

[46] Xie KH, Lu MM, Liu GB. Equal strain consolidation for stone columns reinforced foundation. Int J Numer Anal Met 2009;33(15):1721-1735.

[47] Yuan J, Hicks MA. Large deformation elastic electro-osmosis consolidation of clays. Comput Geotech 2013;54:60-68.

[48] Zhang N, Shen S, Wu H, Chai J, Xu Y, Yin Z. Evaluation of effect of basal reinforcement under embankment loading on soft marine deposits. Geotextiles and Geomembranes 2015;43(6):506-514.

[49] Zhou W, Hong HP, Shang JQ. Probabilistic design method of prefabricated vertical drains for soil improvement. J Geotech Geoenviron 1999;125(8):659-664.

Table 1 Parameters for the numerical simulation followed by Rixner et al. 1986

Undisturbed zone	Density (g/cm^3)	2
	Modulus of elasticity (kPa)	1000
	Poisson ratio	0.35
	Permeability (m/s)	2×10^{-9}
	Void ratio	1.5
Smeared zone	Density (g/cm^3)	2
	Modulus of elasticity (kPa)	1000
	Poisson ratio	0.35
	Permeability (m/s)	1×10^{-9}
	Void ratio	1.5

Table 2 Parameters for the subsoil followed by Chai et al. 1995

Layer	H (m)	γ (kN/m^3)	e_0	C_c	OCR	k_h (10^{-8}m/s)	k_v (10^{-8}m/s)	C_h (m^2/d)	C_v (m^2/d)
B	1.0	15.0	2.0	0.58	5	11.45	7.6	0.1	0.067
AC1	2.8	14.5	2.0	1.0	2	5.7	3.8	0.08	0.053
AS1	1.3	15.5	1.8	0.1	1.2	290	290	54	54
AC2	15.0	14.5	2.5	2.0	1.2	2.64	1.76	0.045~0.087	0.03~0.058
AS2	2.5	16.0	1.7	0.1	1.2	290	290	178	178
AC3	1.5	16.0	1.75	0.7	1.2	2.64	1.76	0.26	0.173

Note: Layer B is the top weathered crust. Layers AC1, AC2, and AC3 are soft clay layers. Layers AS1 and AS2 are sand layers. H is the thickness of the layer. γ is unit weight. e_0 is initial void ratio.

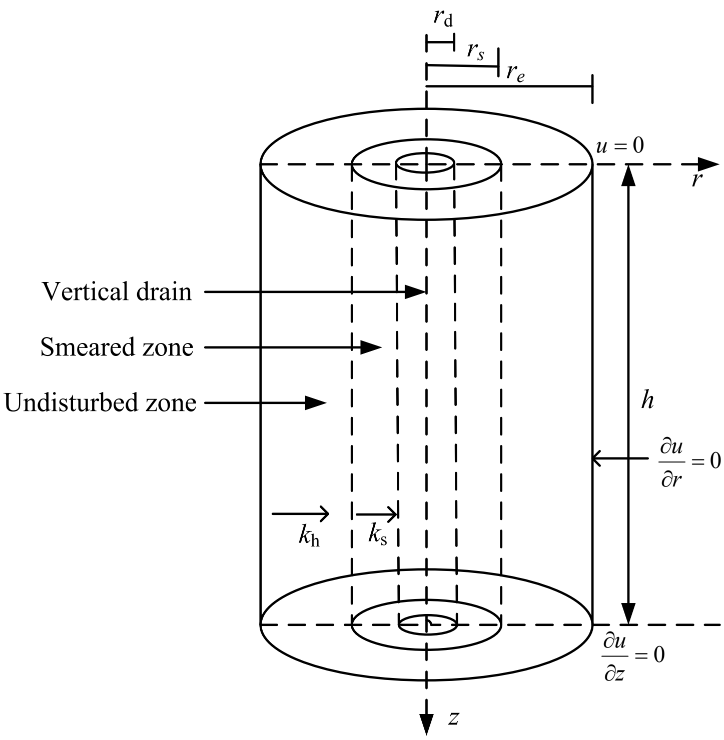

Figure 1 Schematic diagram of axisymmetric consolidation model

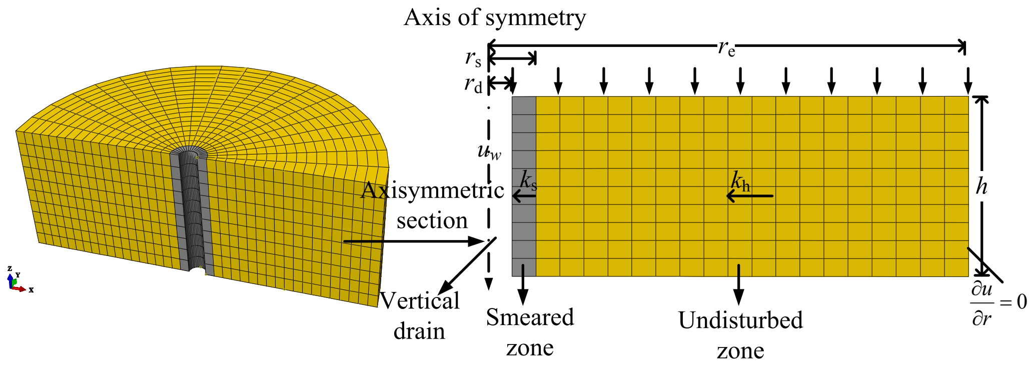

698

699 Figure 2 Schematic diagram of the axisymmetric consolidation model for numerical simulation

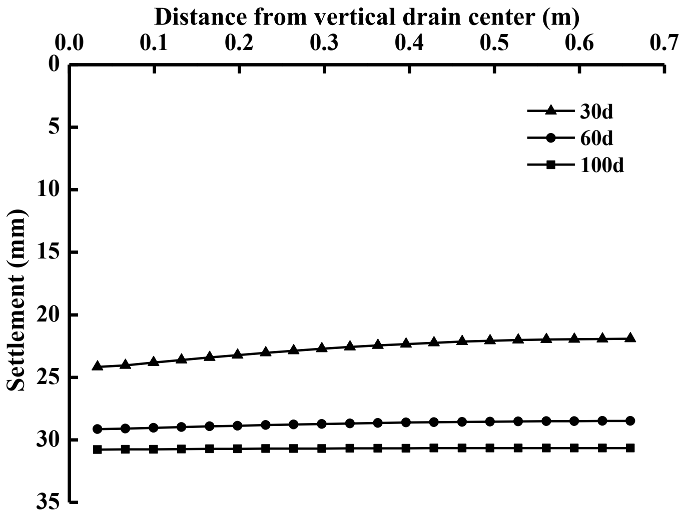

Figure 3 Settlement versus distance *r* from the center of the vertical drain

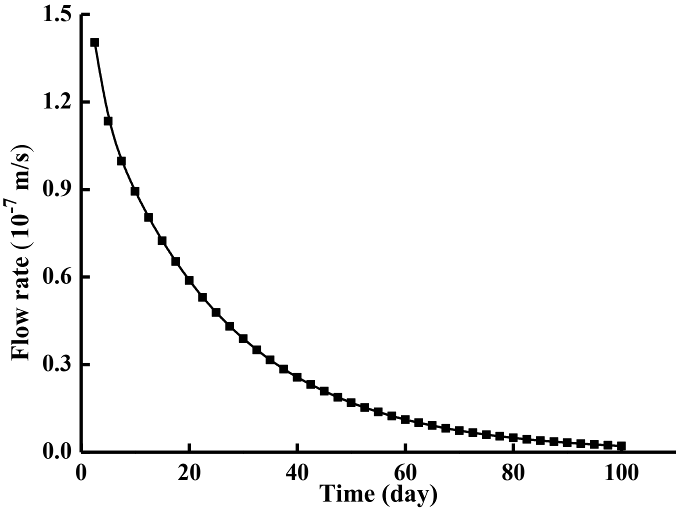

Figure 4 Flow rate versus time

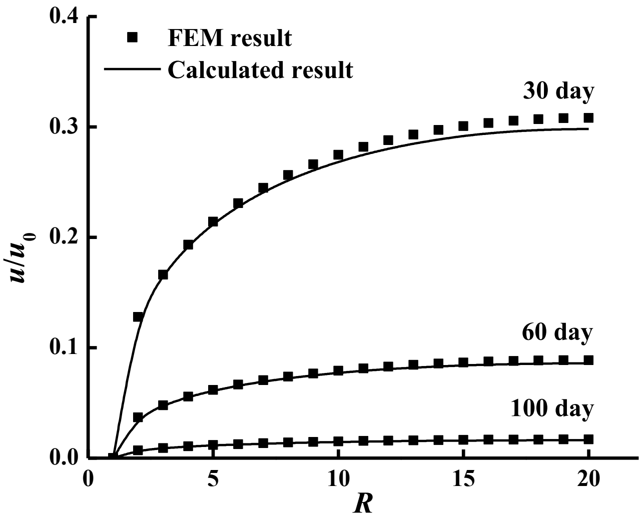

Figure 5 Comparison of u_0/u_0 between the FEM and calculated result

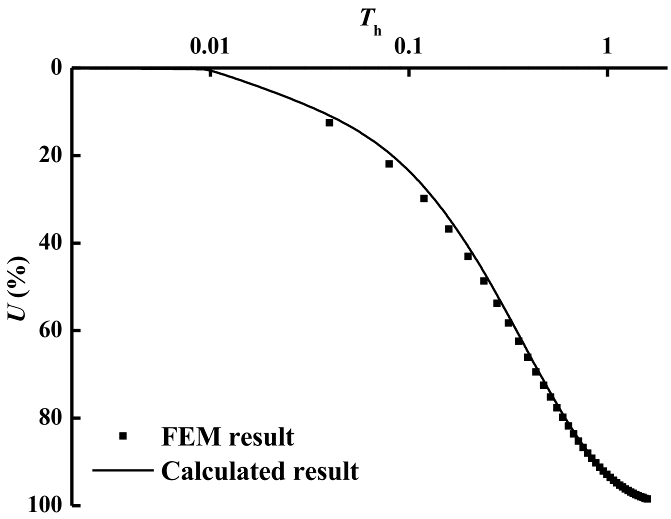

Figure 6 Comparison of DOC between simulation and calculated results

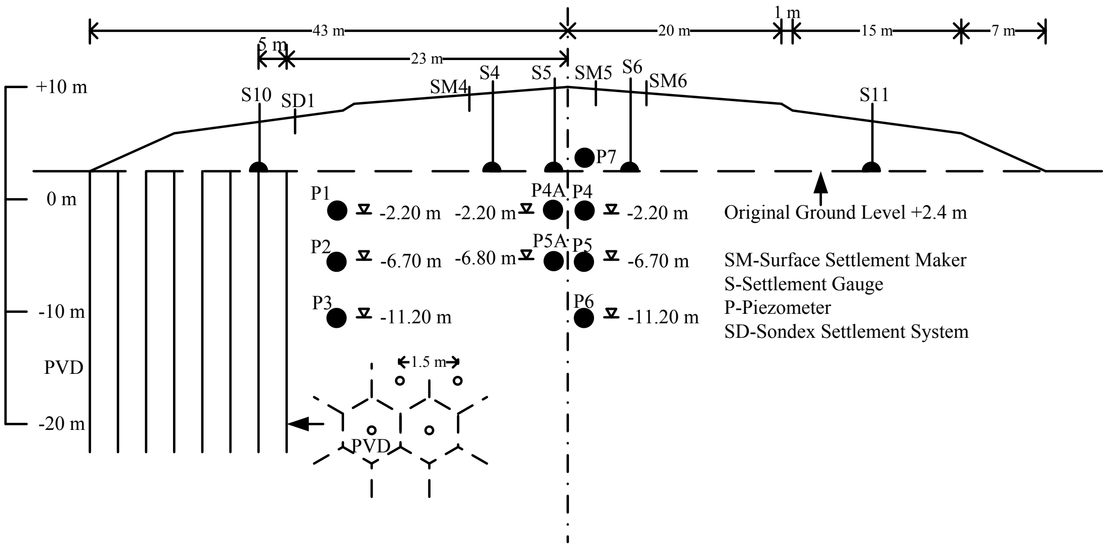

Figure 7 Cross-section of embankment and field instrumentation locations followed by Chai et al. 1995

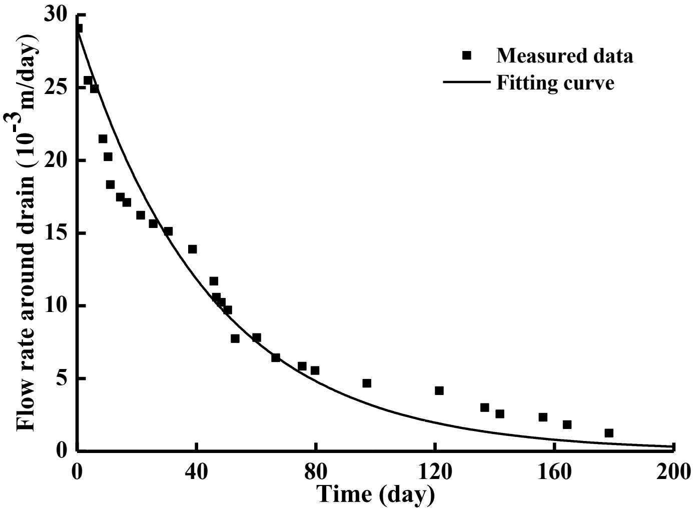

Figure 8 Flow rate measured in the field

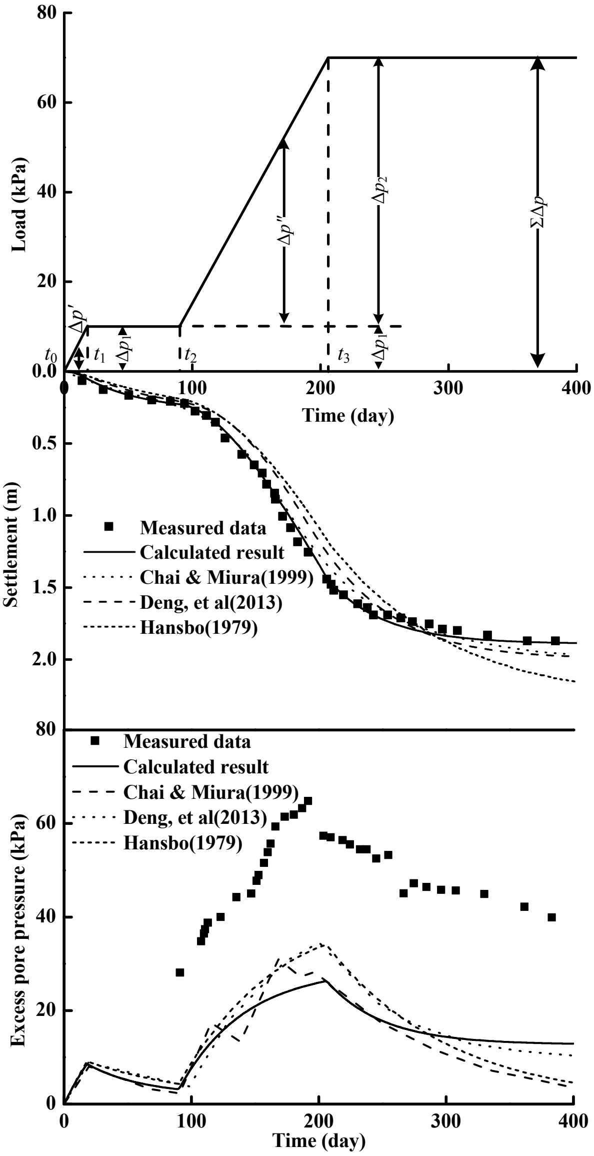

Figure 9 A comparison of settlement and EPWP

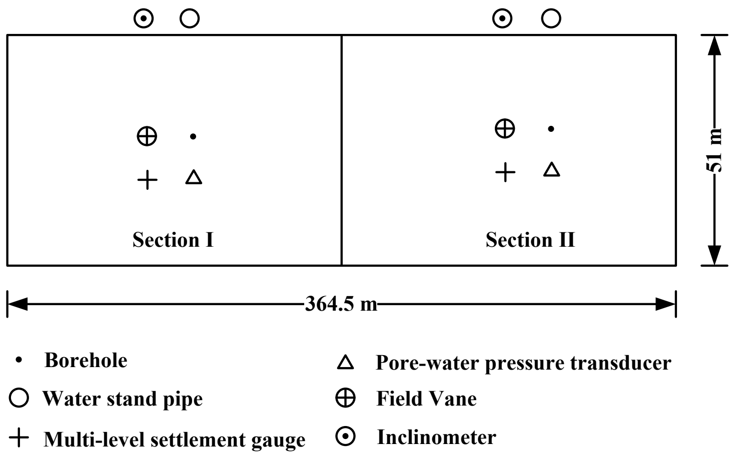

Figure 10 Project site and plan view of instrumentation followed by Chu and Yan 2005

717
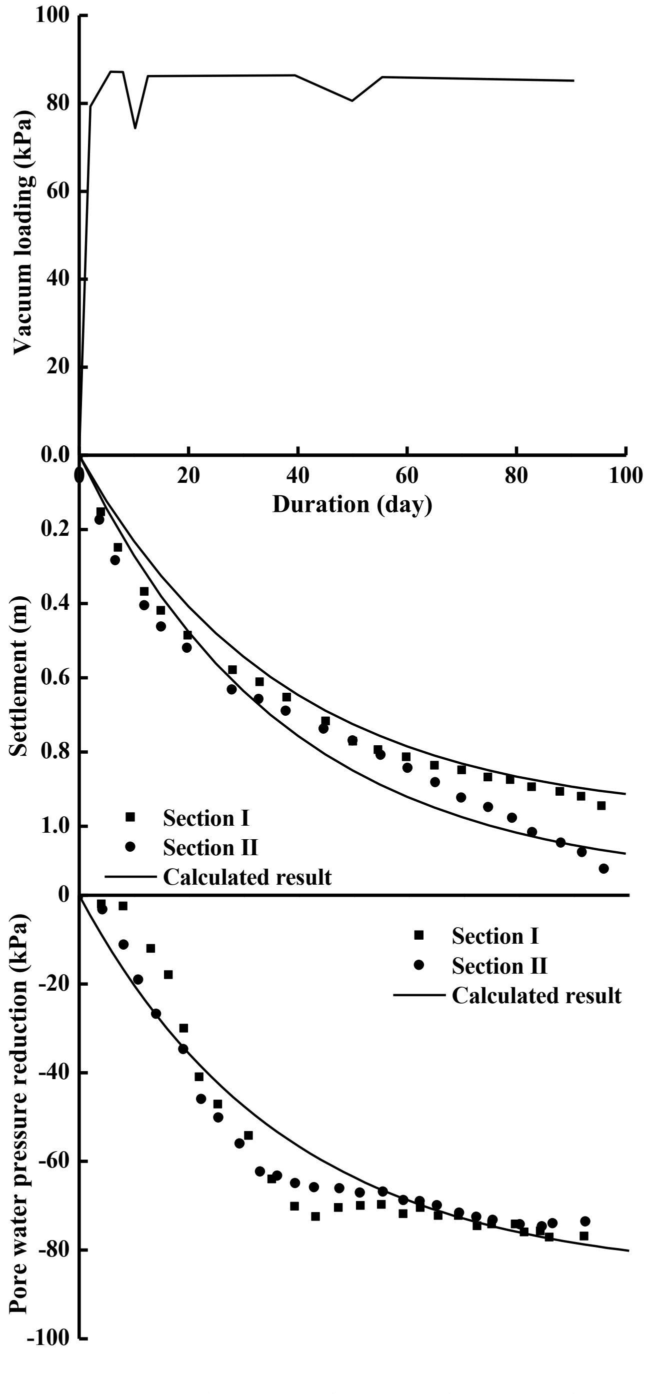

718 Figure 11 Comparison of settlement and EPWP reduction

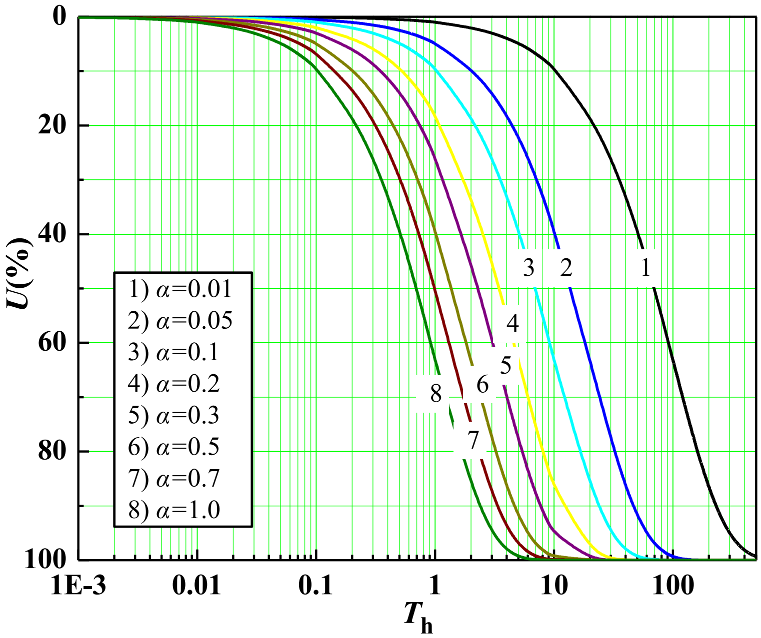

Figure 12 DOC – time factor curve

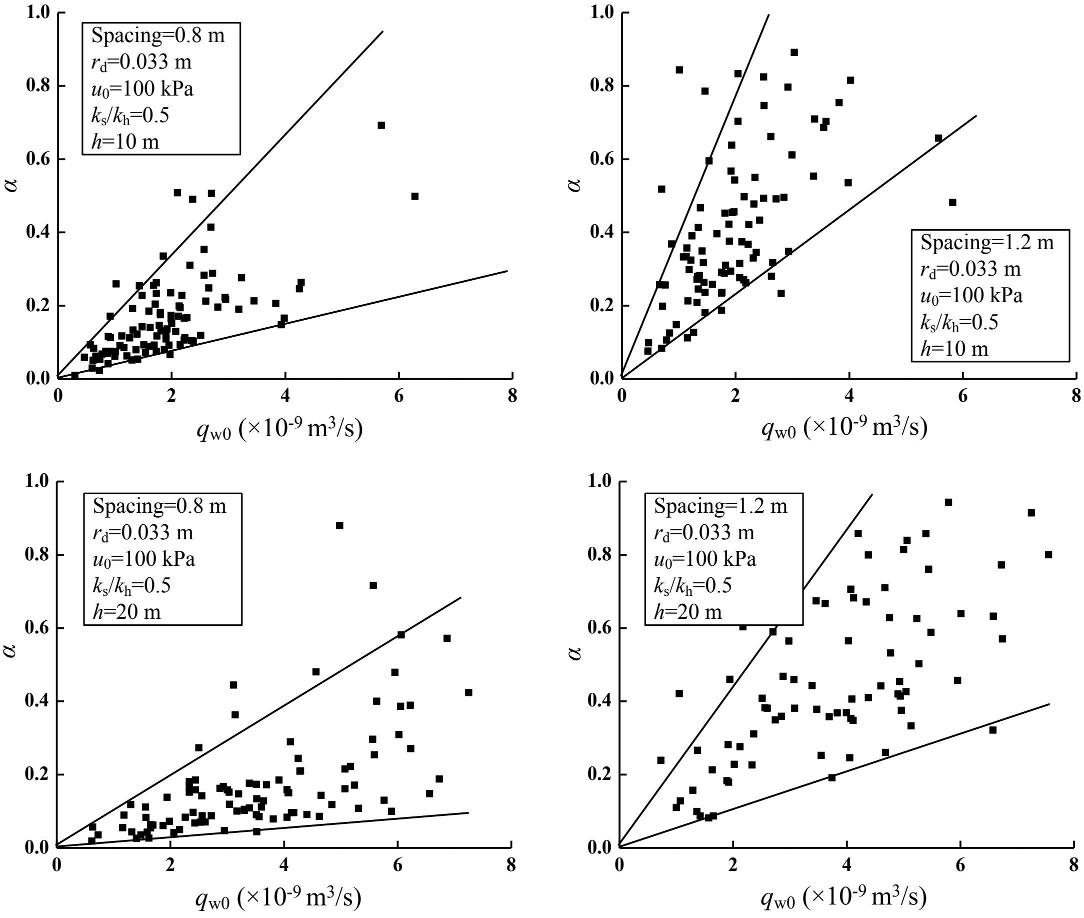

Figure 13 Distribution of α for PVDs arranged in a triangular pattern

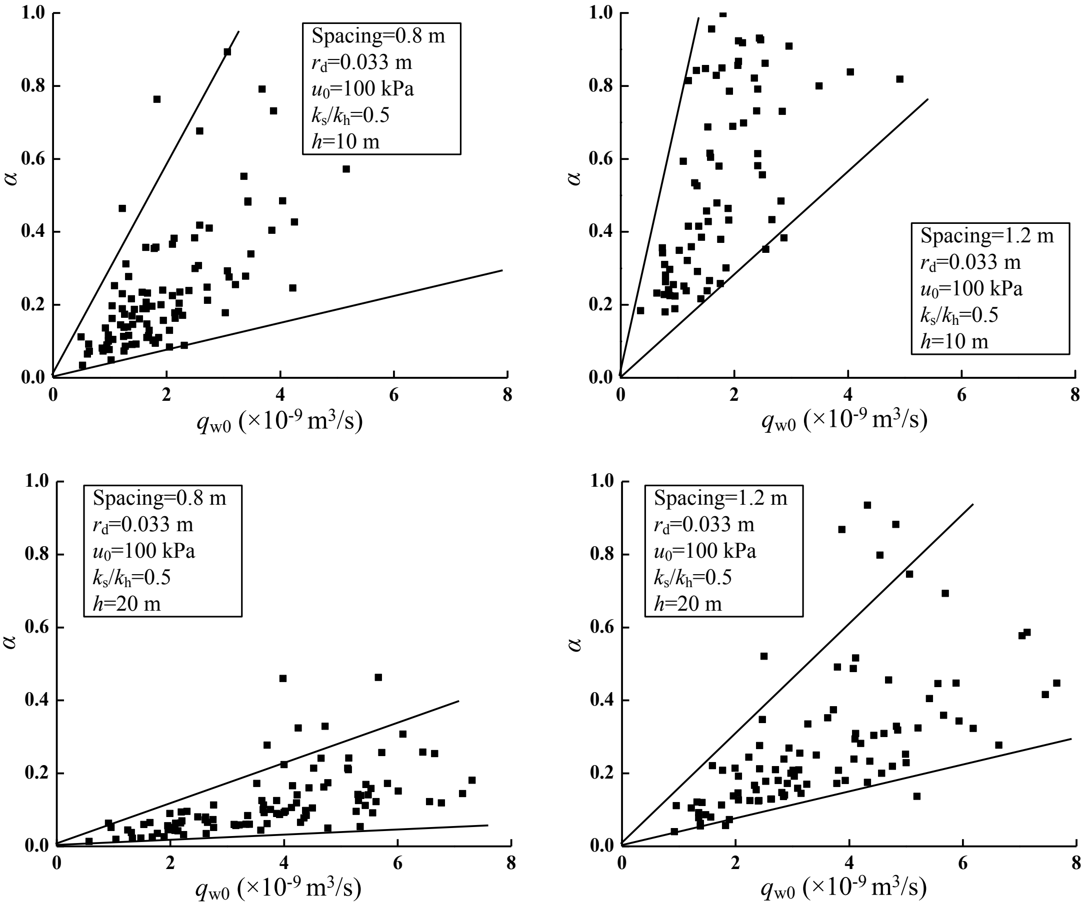

Figure 14 Distribution of α for PVDs arranged in a square pattern